

Composition and Paragenesis of Daqingshanite from the Kamthai Carbothermalite, Rajasthan, India.

Roger H Mitchell

Department of Geology, Lakehead University, Thunder Bay, Ontario, Canada P7B 5E1

[rmitchel@lakeheadu.ca](mailto:rmitchel@lakeheadu.ca)

### Abstract

Daqingshanite in the Kamthai REE deposit (India) occurs as two paragenetic types: primary granular coarse grained crystals coexisting with primary carbocearnite, barite and bastnäsite; and as aligned micro-ovoid globules within clasts of Sr-bearing calcite. Carbocearnite forming trellis-type lamellae in some of these calcite clasts do not represent exsolution and are considered as replacement textures as they formed subsequent to daqingshanite. The origins of the textural relations of the microglobules of daqingshanite to their host Sr-calcite cannot be unambiguously determined, although an exsolution origin is not considered feasible. The textures are similar to those of “chalcopyrite disease” and as such could be interpreted as replacement features formed in a low temperature carbothermal environment which should facilitate replacement. Given that daqingshanite is an early crystallizing phase it is also possible that cotectic crystallization with Sr-calcite occurred, followed by subsolidus re-equilibration with recrystallization along specific crystallographic planes in the calcite. The Kamthai REE deposit is best described as a low temperature carbothermalite microbreccia consisting of a wide variety of clasts resulting from the autobrecciation of rocks formed during, and after, the magmatic to carbothermal transition of an undetermined parental calcite carbonatite-forming magma. Many clasts have been replaced by late stage La-enriched carbothermal fluids mixed with exogenous water during the final low temperature stage of evolution of the deposit.

**Keywords:** carbonatite, carbothermalite, daqingshanite, carbocearnite, britholite, Kamthai, Rajasthan

### Introduction

The mineral subsequently known as daqingshanite was initially described as unknown mineral UK44 from the Mont Saint-Hilaire intrusion in 1976 but could not be formally named due to the absence of a crystal structure determination. Eventually, this rare Sr-REE-P-bearing carbonate, was described and named from the Bayan Obo ore deposit by Yingchen et al. (1983). The mineral was further recognised in the Kamthai “carbonatites” associated with the Samu-Dandhali alkaline complex, Rajasthan, India by Wall et al. (1993); an occurrence confirmed by



Mineralogical Society

This is a 'preproof' accepted article for Mineralogical Magazine. This version may be subject to change during the production process.

DOI: 10.1180/mgm.2024.18

R.H.Mitchell as noted in Bhushan and Kumar (2013) and Bhushan (2015). A further important discovery in the Nkombwa Hill carbonatite (Zambia), which eventually resulted in an accurate crystal structure determination, was reported by Appleton et al. (1992). Daqingshanite was found in the calcite-bearing groundmass of the Sover lamproite by Mitchell (1996) and recently the mineral has been recognized in the Kangankunde (Malawi) and Monteverde (Angola) fenites (Dowman et al. 2022; Amores-Casals et al. 2023) and the Sheep Creek REE deposit (Montana) by Risedorf (2023).

The crystal structure of daqingshanite from Bayan Obo and Nkombwa Hill was determined by Ximen and Peng (1985) and Hughes and Yunxiang (1994), respectively. The high precision crystal structure refinement of Hughes and Yunxiang (1994) established that the mineral was composed of alternating layers of  $\text{Sr}_3\text{REE}_1$  and  $(\text{CO}_3)_3(\text{PO}_4)_1$  resulting in a general formula which can be expressed as  $A_3B_1C_1(\text{CO}_3)_3$  where:  $A = (\text{Sr}, \text{Ca}, \text{Ba}, \text{Na}, \text{K})$ ;  $B = (\text{La-Lu})$ ;  $C = (\text{P}, \text{S})$ .

The primary objective of this contribution is to provide new data on the composition and paragenesis of daqingshanite from Kamthai as this mineral has not been described, or discussed, in any of several recent publications (Patel 2023a,b; Upadhyay et al., 2021) concerned with the geology and mineralogy of this occurrence. *It is not an objective of this work to provide a comprehensive petrogenetic model for the Kamthai REE occurrence and its relationships to the silicate rocks of the Sarnu-Dandhali complex, although some broad genetic relationships are considered on the basis of the evidence obtained in this study.* Aspects of carbonatite nomenclature relevant to the Kamthai occurrence are described below.

#### **Terminological Note: Carbothermalites**

The carbonate rocks at Kamthai, following the initial descriptions by Bhushan and Kumar (2013), have been described in all subsequent publications (Patel 2023a,b; Upadhyay et al., 2021) as carbonatites (*sensu lato*) However, these rocks are actually better described as *carbothermalites* following the criteria proposed by Mitchell (2005) and Mitchell and Gittins (2022), as they are composed of a complex assemblage of carbocearnite, bastnäsite, ancyllite, barite and strontian calcite and other minerals which are all formed at low temperatures from *carbonate-dominated fluids* subsequent to the magmatic to carbothermal transition of the parental magma (see below).

The use of the term carbothermal is preferred in this work, rather than carbonatite, as it describes a mineral assemblage dominated, with respect to the anions, by carbonates, fluorocarbonates, fluorides and sulphates rather than water-rich minerals. The term “carbothermal solution” was used initially by Wall and Mariano (1996, p.197) to refer to “late carbonatites” enriched in rare earth elements (REE). Subsequently, Zaitsev et al. (1998, p.248) recognized “carbohydrothermal” fluids as forming the REE-Sr-Ba carbonate minerals in the Khibiny carbonatites. Wall and Zaitsev (2004, p.347; their Fig.10.1) presented a summary of compositional relations between common REE-Sr-Ba minerals, monazite and apatite in “carbonatites” from which it is clear that occurrences dominated by REE-fluorocarbonates, carbocearnite, and burbankite represent assemblages formed from fluids with high carbonate/water ratios. Note that many investigations of REE-Sr-Ba mineralization associated with alkaline rock complexes simply use the term “hydrothermal” without consideration of the character of the mineral assemblages present. This approach can lead to assemblages dominated by water-poor REE-Sr-Ba carbonates being incorrectly

termed “hydrothermal” deposits. Consequently, Mitchell (2005) and Mitchell and Gittins (2021) recognized that there can be continuum between carbonate and water enriched residual magma/fluids, and that these can be described as carbothermal, carbohydrothermal, or hydrothermal depending on the carbonate/water ratios. In addition it is recognized that carbothermal fluids can evolve in some instances to *bona fide* hydrothermal fluids. Given that the principal REE-Sr-Ba mineral assemblage found at Kamthai is dominated by calcite, carbocernaite and daqingshanite, the term carbothermalite is used in this work to distinguish these rocks from earlier formed magmatic apatite calcite carbonatites (see the discussion section below).

### Geological Occurrence

The Kamthai Rare Earth Deposit (25°44'N: 71°52'E) is a member of the Tertiary Sarnu-Dandhali nepheline syenite-phonolite complex located in the Barmer District of Rajasthan. The geology of this complex is not well-known because of the extensive cover of the outcrops by the windblown sands of the Thar Desert. Aspects of the geology have been described by Bhushan (2015) and Bhushan and Kumar (2013) which indicate that, at the current level of exposure, the complex consists of a large body of nepheline syenite, small intrusions of ijolite breccia, scattered intrusions of the “carbonatite complex”, and numerous thin phonolite dikes. The latter cross-cut the carbonatite complex and an outcrop of ijolite but are older than the nepheline syenite. The “carbonatite complex” consists of an initial irregular intrusion of calcite carbonatite and numerous thin younger Ba-Sr-REE enriched carbonate dike-like intrusions. The latter also occur as isolated irregular dikes which cross-cut an ijolite intrusion.

Although the Kamthai REE-vein deposits are associated geographically with alkaline silicate rocks, interpretation of their relationships and genesis is hindered by the very poor exposure and paucity of petrological investigations. Clearly, the Sarnu-Dandhali alkaline complex has similarities with other alkaline rock carbonatite complexes in that they contain ijolites, nephelinites and phonolites, but documentation of the exact relationships with potential carbonatite-forming magmas such as nephelinite are not available. Recently, Mahala and Ray (2022) have determined that the Sr and Nd isotopic compositions and ages of the alkaline rocks and carbothermalites are similar and concluded that they are probably genetically related. However, Mahala and Ray (2022) did not provide any genetic model apart from some generalizations considering all the rocks to be related by either fractional crystallization or liquid immiscibility.

The Kamthai REE deposit is notable for the presence of abundant carbocernaite, britholite, Sr-barite, strontianite and rare earth element carbonates enriched in La: i.e. bastnäsite-(La), ancylite-(La). The presence of daqingshanite at Kamthai was initially recognized by Wall et al. (1993), who illustrated small (c.10 x 50 microns) anhedral crystals associated with later-forming carbocernaite. Daqingshanite-bearing rocks which have not been subjected to extensive secondary carbohydrothermal alteration in terms of their modal mineralogy are best termed barite bastnäsite carbocernaite carbothermalites (see below). Note that Patel et al. (2023b) provided a paragenetic sequence for the carbothermalites which inexplicably does **not** include daqingshanite.

Standard optical and BSE-petrographic observations (this work; Bhushan, 2015; Patel et al., 2023a,b) show clearly that the Kamthai REE carbothermal vein deposit, referred to as a “late carbonatite” by Wall and Mariano (1996), as a whole does not exhibit the typical textures or mineralogy of primary magmatic carbonatites as defined by

Mitchell and Gittins (2022). However, such carbonatites form the irregular earlier calcite carbonatite plug and occur as clasts within the REE-enriched carbothermal deposit. The latter is here considered as a carbothermal microbreccia consisting of veins and clasts with a wide range of textural and mineralogical characteristics.

The Kamthai carbothermalites (*sensu lato*) are fine grained microbreccias which exhibit extra-ordinarily complex dissolution, re-precipitation and secondary replacement textures. Data given by Patel et al. (2023a) show that Kamthai calcite exhibits a very wide range of textural and compositional types that actually cannot always be placed objectively in any simple paragenetic sequence, although they suggest that there is a broad division between “magmatic” and “hydrothermal” assemblages. These have been described by Patel et al. (2023a,b) and Upadhyay et al. (2021), who claim that diverse “primary” and “secondary mineral assemblages” can be recognized. Primary assemblages are considered by Patel et al. (2023b) to include Sr-bearing calcite (3-12 wt.% SrO) termed “magmatic calcite” although this interpretation appears to include magmatic and carbothermal calcite compositions, and is based upon the incorrect assumption that all primary calcite must be Sr rich. However, given that most of the calcite in the carbothermalite breccias do not have the allotriomorphic granular textures or compositional features of the low Sr contents of *bona fide* magmatic calcite these are best described as carbothermal calcite. Note that some of the carbothermal calcite investigated in this work would be considered as “magmatic” by Patel et al. (2023a,b).

### Analytical Methods

Polished thin sections of nine grab samples of carbothermal microbreccia provided by Ramgad Minerals were examined by back-scattered electron petrography as standard optical petrographic methods are not suitable for these fine grained texturally-complex materials. Compositions of the phases present were determined by *quantitative* energy dispersive X-ray spectrometry using a Hitachi FE-SU70 scanning electron microscope equipped with an Oxford Instruments X-MAX 80mm<sup>2</sup> Si-drift detector and the AZtec software package. The electron accelerating voltage was 20 kV and the beam current 300 pA. Standards used were: wollastonite (Si,Ca); corundum (Al); jadeite (Na,Al); BaF<sub>2</sub> (Ba,F); Mn-hornblende (Mg, Fe, Si, Mn); synthetic rare element phosphates (La, Ce, Pr, Nd, Sm, P); SrTiO<sub>3</sub> (Sr, Ti); ThNb<sub>4</sub>O<sub>12</sub> (Th, Nb); ilmenite (Ti, Fe). The rastered beam (15x15 micron) and low beam currents (300pA) employed for quantitative X-ray energy dispersive spectrometric analysis permitted accurate and reproducible analysis of small crystals in a variety of hosts without excitation of the latter. Note that the brightness and contrast settings of BSE-detectors are critical in distinguishing daqingshanite from associated carbocernaite and britholite.

It is important to note that analysis of alkali-REE-carbonates requires that a low beam current coupled with rastering of the analytical site must be employed if alkali loss is to be avoided. Supplementary Fig.1 demonstrates that spot analyses of carbocernaite for a live time of 60 s (30% dead time) with a 300pA beam current, results in significant beam damage whereas rastering causes no obvious damage during the same irradiation time. Several spot analyses resulted on average in a 61% decrease in the Na content of the carbocernaite whereas there was no change in the Na content for a 15 x 15 micron area with rastered analysis. Similar effects were observed for the analysis of ancylite. It is well-known that analysis of carbocernaite by EMPA methods requires electron beam defocussing to about 10 microns

to avoid Na loss with beam currents of 20nA (Chakhmouradian et al. 2017). From these observations and the above it is apparent that the compositions of carbocearnite given by Patel et al; (2023a) using a 50nA beam current, even with defocussing (1-15 microns), reflect significant alkali loss resulting in significant A-site cation deficiencies. Hence, Na<sub>2</sub>O contents reported by Patel et al. (2023a) range from 0.1-2.8 wt.%; i.e considerably less than typical carbocearnite compositions which vary from 2.5-5.4 wt. Na<sub>2</sub>O, with the majority in the range of 3-5 wt.% (Wall et al.,1993; Zaitsev et al., 1998; Chakhmouradian et al., 2017; Sitnikova et al., 2021).

### **Daqingshanite Paragenesis and Composition**

Daqingshanite in some of the Kamthai carbothermalites, which have not been subjected to extensive later carbohydrothermal alteration, occurs in two textural-paragenetic types: (1) anhedral coarse grained primary crystals associated with britholite, carbocearnite and barite; (2) very small ovoid-to-round microcrystalline inclusions in Sr-rich calcite clasts, which in some instances, are characterized by trellis-textured lamellae of carbocearnite occupying the rhombohedral cleavage planes of the calcite.

#### *Paragenetic Type 1 - paragenesis*

Figure 1 illustrates the typical paragenesis of daqingshanite which occurs as abundant anhedral-to-rounded crystals surrounded by large interlocking anhedral crystals of carbocearnite, commonly with associated contemporaneous barite and bastnäsite (see below). The daqingshanite contains rounded inclusions of britholite and rarer monazite-(La). Figure 2 illustrates clusters of anhedral large daqingshanite crystals of variable composition which have crystallized prior to carbocearnite. The late-forming matrix is strontian calcite of diverse composition (8-12 wt.% SrO). Britholite is present as earlier-formed rounded inclusions in daqingshanite. Figure 3 shows daqingshanite which has apparently crystallized in association with ancylite together with oscillatory zoned Ca -Fe-Mn carbonate (14-29 wt.% FeO; 19-31 wt.% MnO; 9-13 wt.% CaO). Daqingshanite also occurs as anhedral single crystals within the strontian calcite matrix. These are interpreted to represent material derived by the disaggregation of previously formed aggregates of daqingshanite crystals.

#### *Paragenetic Type 1 Composition*

Typically, Kamthai daqingshanite is enriched in the light rare earth elements (REE) although these are not dominant over Sr. No data are available for the heavy REE or other trace elements. Hughes and Yunxiang (1994) consider that there is little or no substitution of hydroxyl ions or fluorine in the structure. Supplementary Fig. 2 illustrates the composition of Kamthai daqingshanite as determined by energy dispersive X-ray spectrometry which shows clearly the presence of Na, K and S and the absence of Cl. Although a small peak attributable to F K $\alpha$  is also present this cannot be resolved using SEM-EDS to give a satisfactory analytical accuracy or precision due to significant overlaps with low energy REE and oxygen peaks. It is estimated using 120 seconds counting times that F is present near the limits of detection at contents of 0.3-0.4 wt.%. These amounts are insignificant with respect to the structural formulae of daqingshanite calculated on the basis of three carbonate groups.

The composition of Kamthai daqingshanite was initially established by Wall et al. (1993) who noted the significant differences to the type locality material from Bayan Obo which is significantly enriched in Ba (Table;

comp.9), has lower REE contents and that S is present (Table 1; comp.8). Although Appleton et al. (1992) did not determine the S content of Nkombwa daqingshanite, their data (Table 1; comp.8) included F (0.29 wt%) and Cl (0.10 wt%).

Figure 4 shows examples of the compositional zoning of Kamthai daqingshanite as illustrated by back-scattered electron (BSE) imagery. Simple core-to-rim variation is not evident in the majority of the crystals although instances of internal compositional gradients are evident. These, and the well-defined compositional boundaries, within other parts of the crystal are attributed to sector zoning. Representative compositions of the zones are given in Table 1. Those with high BSE-contrast (dark orange in Figs.2 and 4) are enriched in Sr and P relative to other regions of the crystals with low BSE contrast and are depleted in Ba, Na, K and S, although none of the compositions are as enriched in Sr or Ba as the Nkombwa and Bayan Obo material (Table 1). Primary daqingshanite from the Sheep Creek carbothermalite (Risedorf, 2023) is relatively Ba-rich (4.5-7.1 BaO wt.%) but Sr and REE-poor (26-28 SrO; 9.9-13.5 La<sub>2</sub>O<sub>3</sub>; 11.8-13.59 Ce<sub>2</sub>O<sub>3</sub> wt.%) compared to Kamthai daqingshanite. Daqingshanite from Nkombwa and Sover are Sr-rich, whereas that from Bayan Obo is relatively Ba-rich. From Figure 5 it is evident that daqingshanite can exhibit significant compositional variation especially with respect to Ca, Sr, and Ba contents, and it is suggested that both the Ba and Ca end-member compositions might exist in nature or can be synthesized.

#### *Paragenetic Type 2*

Paragenetic type 2 occurs as very small (typically <10 microns) discrete ovoid globules set in strontian calcite (10-12 wt.% SrO; 2-3 MnO; 0.4-0.5 BaO; ~0.5 MgO) matrices. Two textural varieties are present. In both of these, the daqingshanite globules have a subparallel well-defined orientation that does not follow any obvious crystallographic planes (see below).

In one textural variety (Figure 6a,b), other minerals are rare-to-absent, although single anhedral crystals of carbocearnite, calcian strontianite, daqingshanite, britholite and Al-Mn-bearing magnetite, lacking any preferred orientation relative to the globules can be found (Fig. 6c). BSE petrography demonstrates that these daqingshanite-strontian calcite assemblages represent single clasts set in a strontian calcite matrix that lacks globular daqingshanite (Fig.6a). This cementing calcite is poorer in SrO (7-10 wt.%) and MgO (< 0.3 wt.%) than that of the clasts.

Another type of clast characterized by daqingshanite globules is illustrated in Fig. 7. These are characterized by a network of thin carbocearnite lamellae. In some clasts these lamellae form a trellis-like intergrowth of two sets of parallel lamellae which apparently follow the rhombohedral cleavage of the Sr-calcite host (Fig.7a). *It is to be particularly noted that the orientation of the carbocearnite lamellae is not the same as that of the daqingshanite globules, and that carbocearnite lamellae cross-cut these globules (Fig.7b).* In other clasts, depending upon their orientation, only one set of lamellae is evident, in others flame-like structures emanate from the lamellae (Fig. 8a). In some examples lamellae are curved and/or form symplectite-like intergrowths. The carbocearnite lamellae in some instances contain single crystals of daqingshanite, Al-Mn magnetite, barite and britholite (Fig. 8a). The Sr-calcite (11-12 wt.% SrO) host to all varieties is similar to that of clasts lacking carbocearnite lamellae.

The strontian calcite matrices of both types of clasts also commonly exhibit replacement by many small (< 30

microns) of amoeboid-like fine grained intergrowths (Figs 8a,b). Although these are too small for accurate analysis it is apparent that they consist of Ba-Mn-bearing Sr-calcite (c.28.5 SrO; c.1.0 BaO; 1 % MnO wt.%) intergrown with relatively Sr-poor calcite (c.12 % wt.% SrO) enriched in MgO (0.4 wt.%), MnO (c.2 wt.% and REE (wt.% :0.9 La<sub>2</sub>O<sub>3</sub>; 1.7 Ce<sub>2</sub>O<sub>3</sub>). Patel et al (2023a) describe these as secondary carbocernaite although the crystals in the intergrowths are actually too small for accurate EMP analysis.

#### *Globule Daqingshanite Composition*

Because of their small size determination of the composition of the globules is very difficult due to excitation of the host Sr-calcite. Rare examples with larger size (c. 15-20 microns) can be found which give reasonable rastered analytical totals and P, REE and Sr contents (Table 2). These data indicate that the globules have compositions which are very similar to the granular type 1 daqingshanite. However, even for these crystals, matrix excitation of Ca cannot be ruled out.

#### **Carbocernaite**

##### *Paragenesis*

Carbocernaite, is a major component of the material investigated, and occurs intergrown with daqingshanite as anhedral granular crystals set in a Sr-calcite matrix (Figs. 1-3), large anhedral granular clusters in clasts, and as diverse lamellae in daqingshanite-strontian calcite clasts (Figs. 7,8). BSE-petrography shows that in all cases carbocernaite has crystallized subsequent to daqingshanite but has not pseudomorphed this mineral. Pseudomorphs after burbankite are not present. Isolated anhedral crystals of carbocernaite in diverse matrices represent disaggregated granular aggregates of the type shown in Figure 2. During the formation of lamellae some carbocernaite appears to have transported other minerals (daqingshanite, magnetite, britholite; pyrochlore) along the lamellae. A common assemblage found in the material investigated consists of apparently contemporaneously crystallizing carbocernaite, Sr-barite and bastnäsite-(La). All carbocernaite types appear to have formed prior to the strontian calcite matrices

Carbocernaite is known to occur in carbonatites and/or carbothermalites in a wide variety of textural types: discrete crystals and clusters; supposed exsolution lamellae in calcite; pseudomorphs after burbankite, calcite or ferroan dolomite and overgrowths on cordylite (Chakhmouradian et al. 2017). The bulk of the Kamthai carbocernaite occurs as discrete crystals and overgrowths on daqingshanite and its formation during the early stages of crystallization is unquestionable. The origins of the trellis lamellae carbocernaite are less easily determined and although these have the appearance of trellis exsolution they exhibit features at variance with this process which are discussed below.

##### *Composition*

The structure of carbocernaite has been determined by Shi et al (1982) and Chakhmouradian et al. (2017) and the ideal composition is (Ca,Na)(Sr,Ce,Ba)(CO<sub>3</sub>)<sub>2</sub>. Representative compositions and structural formulae of Kamthai carbocernaite are given in Table 3 which demonstrates, in accord with BSE-imagery (Figs.2-5), that there is very little compositional variation in the material investigated. In contrast to Wall et al. (1993), who report Na-poor lamellae in calcite, there are no significant compositional differences between granular and lamellae carbocernaite. These compositions are very similar to carbocernaite from Khibina (Zaitsev et al. 1998) and Bear Lodge (Chakhmouradian et

al. 2017), all of which have  $\text{La/Ce} < 1$  in contrast to the data of Wall et al. (1993) which have  $\text{La/Ce} > 1$  (Table 3 comp.11) or Patel et al.(2023) for which there are  $\text{La/Ce}$  ratios varying from less than, to greater than, unity. As noted above, all data given by Patel et al. (2023) are deficient in Na, ranging from 0.4-2.8 wt.%  $\text{Na}_2\text{O}$  (Table 3; comps. 9 and 10), and are considered to be inaccurate due to extensive Na loss under the extremely high electron beam currents employed for analysis (see methodology above) and are not discussed further.

### **Britholite**

Britholite  $(\text{REE,Ca,Sr})_5(\text{SiO}_4,\text{PO}_4)_3(\text{OH,F})$  is commonly found as ovoid inclusions in daqingshanite (Fig. 2) and carbocearnite, as aggregates of anhedral crystals in bastnäsite-(La) (Fig.9) and as single anhedral crystals in Sr-calcite which are undoubtedly derived by disaggregation of such aggregates. All britholite is altered and characterized by irregular and heterogeneous regions of different BSE-contrast (Fig.9). Euhedral crystals of britholite are not found and it is evident from the texture that britholite, and monazite, have been resorbed prior to incorporation into all other minerals present in the Kamthai carbothermalites.

Table 4 presents representative compositions of britholite. Regions of high BSE contrast (darker orange in Fig. 9) are enriched in Si and REE relative to regions of low BSE contrast which are relatively enriched in P and Ca. These compositional variations reflect substitutions in the well-known britholite-apatite solid solution series. Although all britholite analysed contains F (0.4-1.0 wt.%), analytical totals are low reflecting the presence of significant amounts of OH (Table 4). Thus, the mineral here is best referred to as hydroxylbritholite. Previous compositional data for Kamthai britholite given Wall et al. (1993) appear to be in error as the structural formula (Table 4; comp.7) indicates significant *A*-site deficiencies and *B*-site excess with *A/B* ratios of 1.3. Patel et al. (2023) have recognized “magmatic” britholite and “altered or secondary” britholite at Kamthai with the latter being similar in composition (Table 4; comp. 9) and texture to the britholite analysed in this work. The trend of compositions from “magmatic” to “secondary” hydroxylbritholite given by Patel et al. (2023) is similar with decreasing Si, REE and F coupled with increasing Ca, P, OH. All britholite analysed in this study have low  $\text{La/Ce}$  ratios (0.48-0.56), whereas Patel et al. (2023) have reported “magmatic” La-enriched types with  $\text{La/Ce}$  ratios of 0.64-0.69 and “altered types” with  $\text{La/Ce}$  ratios of 0.62-0.95

### **Discussion**

The objective of this contribution is not to provide a comprehensive genetic model for the Kamthai REE deposit, rather, the principal intent is to outline some mineralogical and broad textural features which are of genetic significance which have not been considered in previous investigations. Foremost of these is recognition of two textural varieties of daqingshanite i.e. granular and micro-ovoid, and evidence that the deposit is a carbothermal microbreccia formed in a least three genetic stages.

#### *Origins of the Daqingshanite Parageneses*

With respect to the granular type 1 variety of daqingshanite, BSE-petrography demonstrates it has crystallized subsequent to altered britholite and monazite-(La) and prior to abundant carbocearnite (Figs. 1-3). The anhedral-to-ovoid habit and heterogeneous compositions of both daqingshanite (Fig. 3-4) and britholite (Fig.8)



suggest resorption and alteration during transport in the fluids which crystallized the host granular carbocearnite, barite and bastnäsite. These assemblages are set in a matrix of Sr-bearing calcite (Fig.1) and are considered to represent transported and disaggregated clasts within the carbothermal fluids which formed the Sr-bearing calcite. The latter is here not considered to be “magmatic calcite” unlike the suggestion of Patel et al. (2023a,b) on the basis of the high SrO content of the calcite (see below).

The microgranular ovoid -to-globular type 2 daqingshanite is found in discrete sub-angular clasts which in some instances also contain lamellae of carbocearnite (Fig.7). These clasts are set in a relatively Sr-poor calcite (8-10 wt.% SrO) matrix compared to the calcite (11-13 wt.% SrO) which forms the host to the daqingshanite globules. The origins of the daqingshanite globules are clearly distinct from those of the granular variety and their sub-parallel orientation might initially suggest an exsolution origin from their host Sr-calcite. Unfortunately, there are no experimental phase equilibria which are relevant to these compositions. The texture exhibited is similar to that of “chalcopyrite disease”, which consists of micro-globules of chalcopyrite in a sphalerite host (Fig.10). The origins of the texture have been widely debated and ascribed to exsolution, replacement or co-precipitation (Barton and Bethke 1987; Nagase and Kojima 1997; Tun and Aye 2020). These investigations have typically ruled-out exsolution except for high temperature metamorphosed ores and focussed on hydrothermal processes. Exsolution is considered unlikely for the daqingshanite in calcite as the globules, although forming linear arrays, these do not follow the rhombohedral calcite cleavage planes (see below). Nagase and Kojima (1997) have suggested that ellipsoidal chalcopyrite in sphalerite reflects extensive replacement whereas a triangular morphology indicates coprecipitation. On this basis, the daqingshanite globules could be interpreted as replacement features. Clearly, the daqingshanite globules at Kamthai have formed in a low temperature carbothermal environment which should facilitate replacement. Given that daqingshanite is an early crystallizing phase it is also possible that cotectic crystallization with Sr-calcite occurred, followed by subsolidus re-equilibration with recrystallization along specific crystallographic planes in the calcite. Until further HRTEM investigations are undertaken the origins of the globular daqingshanite texture will remain enigmatic.

Some clasts containing microgranular daqingshanite globules are also characterized by trellis-like lamellae of carbocearnite (Fig.7). These lamellae follow the rhombohedral cleavage of the calcite host and thus have morphological similarities with the trellis exsolution of ilmenite in magnetite (Haggerty 1996). Both Wall et al. (1993) and Patel et al (2023,ab,) attribute the Kamthai trellis texture to exsolution of carbocearnite from a pre-existing Ca-Sr-Na-REE-carbonate solid solution. However, BSE imagery shows that the carbocearnite actually appears to have invaded the existing daqingshanite-calcite assemblage as carbocearnite lamellae can be seen clearly to cross-cut daqingshanite globules (Fig.7b). The lamellae in some instances are not continuous and can also develop flame-like protrusions into the host calcite (Fig. 8), with symplectite-like intergrowths being developed in some cases. Regarding exsolution, it would seem highly improbable that exsolution of daqingshanite followed by a second exsolution of carbocearnite would occur. Further evidence for a replacement origin is that some carbocearnite lamellae contain small anhedral crystals of britholite, daqingshanite, barite, and Mn-Al-bearing magnetite. These early-forming minerals (or antecrysts) appear to have been transported along the lamellae during their emplacement (Fig.8). It is

apparent that trellis carbocearnite is present only in some of the globular daqingshanite-bearing clasts and that both textural types of clast can occur juxtaposed. This observation implies that all of the globular daqingshanite-bearing clasts were formed at the same time, but only some were transported to an environment where carbocearnite-forming fluids were available to enter the calcite cleavage planes. Note that subsequently both types of clast were subjected to secondary replacement processes as illustrated in Fig 8b and that these were more intense in the clasts characterized by trellis lamellae. All clasts were subsequently mixed and cemented by Sr-calcite. In summary, it is proposed that the trellis-like carbocearnite-bearing clasts were not formed by exsolution and a replacement origin during transport is proposed.

#### *Carbothermalite microbreccia formation*

Standard optical and BSE-petrographic observations (this work; Patel et al., 2023a,b) show clearly that the Kamthai REE deposit as a whole does not exhibit the typical textures or mineralogy of primary magmatic carbonatites as defined by Mitchell and Gittins (2022). Such carbonatites are present only as clasts (see below) within the deposit, which is actually a breccia consisting of veins and clasts with a wide range of textural and mineralogical characteristics. Many of the earlier-formed clasts have been subjected to low temperature secondary replacement processes (Uphadyaya et al., 2021).

The Sarnu-Dandhali complex is similar to other subvolcanic nephelinite-phonolite complexes, such as Freemans Cove (Mitchell and Platt, 1984), Balcones (Barker et al., 1987) and Hegau-Urach (Engelhardt and Weiskirchner, 1963), although REE deposits have not been found associated with these complexes. Unfortunately, plutonic members of the Sarnu-Dandhali complex are not well-exposed. The observations of Bhushan and Kumar (2013) have shown that the “carbonatite plug” and the REE-enriched veins at Kamthai are geographically associated with cross-cutting younger phonolite dykes but there are no evident genetic relationships with these subvolcanic silicate rocks. As a direct mantle origin for these carbothermalites is extremely unlikely, it is highly probable that the REE-rich veins are derived from unexposed late stage differentiates of plutonic members (ijolite suite rocks) of the complex. Evidence in support of this hypothesis is the occurrence of one Ba-rich carbonate dike intruding an ijolite breccia. Further geological and geophysical exploration of the area is obviously required.

From these observations it is proposed that the deposit formed in at least three stages: (1) formation of magmatic calcite carbonatite by fractional crystallization of an as yet undetermined parental magma in a plutonic environment; (2) differentiation of the calcite carbonatite-forming magma to low temperature carbothermalite-forming vein deposits coupled with autobrecciation; (3) formation of late stage veins and replacement of pre-existing clasts by “secondary” LREE-enriched carbothermal fluids mixed with exogenous water. The paragenetic sequence and major mineral assemblages associated with the three stages are summarized in Figure 11.

The genetic model is similar to the common magmatic to hydrothermal transition proposed to explain the genesis of ore deposits associated with plutonic granitoids such as porphyry copper deposits (Audétat and Edmonds 2020) or critical metal-bearing peralkaline granites (Ronchi et al. 2011). This model considers that crystallizing plutons reach fluid saturation during crystallization of the parental magma with subsequent continuous separation of low temperature hydrothermal fluids which are commonly accompanied by brecciation. A similar model for “late-forming”

REE deposits associated with alkaline rock carbonatite complexes has been suggested by Wall and Mariano (1996) and Wall and Zaitsev (2004). The magmatic-to-carbothermal transition proposed by Mitchell and Gittins (2022) is an analogous process involving carbonate-rich fluids rather than hydrothermal fluids.

Stage 1 is represented by clasts of coarse grained magmatic calcite carbonatite which contains accessory fluorite, magnetite and minor dolomite (Fig.12). Calcite in these clasts ranges in texture from allotropic granular to prismatic laths. These calcite are enriched in MnO (4-5 wt.%) and poor in SrO (1-2 wt.%) relatively to carbothermal calcite. The presence of interstitial late stage miarolitic cavities, which are not secondary replacement features, containing intergrowths of carboceomite, barite and ancylite demonstrates that carbothermalite-forming fluids were present in the later stages of crystallization of the calcite carbonatite-forming magma (Fig.12), and that REE enrichment is a primary fractional crystallization process. Other clasts representing stage 1 material are pyrochlore-apatites (Fig.13) similar to those found in magmatic carbonatites at Good Hope, St. Honoré and Panda Hill (Mitchell et al., 2022). This observation suggests that apatite forms only in stage 1 and primary britholite probably also crystallized at this time (700-900°; Mollé et al. 2021). Thus, the sequence of P-bearing minerals at Kamthai is apatite → britholite → daqingshanite. Clasts containing abundant magnetite as suggested by Uphadyay et al (2021) do not appear to be common.

Stage 2 represents brecciation of stage 1 calcite carbonatites by several generations of granular type 1 daqingshanite-carboceomite carbothermalite-forming fluids formed during the initial stages of the magmatic to carbothermal transition. Type 2 daqingshanite-bearing rocks formed at this time and these were also fragmented by the continuing evolving fluids, resulting in auto-brecciation and cementation of all of these diverse clasts in residual Sr-calcite forming fluids (Fig. 7). Stage 3 represents residual carbothermal fluids undergoing further evolution and becoming enriched in La relative to Ce and other REE together with the mixing of exogenous water enriched in O<sup>18</sup> as shown by Uphadyay et al. (2021). These fluids, which can be considered as carbohydrothermal fluids (Mitchell, 2005) invaded, and altered pre-existing breccias, created new breccias and deposited a wide variety of Mn and Fe bearing carbonates together with La-enriched REE fluorocarbonates such as bastnäsite-(La) (Fig.14).

An important conclusion of the above model is that the bulk compositions of none of the rocks forming the Kamthai REE deposit represent liquid compositions and that the heterogeneous mineral assemblages present cannot represent equilibrium assemblages. Hence attempts to reconstruct the “hydrothermal fluid composition” as attempted by Patel et al. (2023a) are not realistic. In addition, the partition coefficients of Chebotarev et al. (2022) used by Patel et al. (2023a) were derived from melt compositions that were highly enriched in Na<sub>2</sub>O (mainly 20-26 wt.%) and formed at temperatures of 650-900°C i.e. well above those expected for the magmatic to carbothermal transition (<400°C) and stability of Na-REE-Sr carbonates (i.e.100-500°C Perry and Gysi 2018; Louvel et al. 2022).

## Conclusions

1. The Kamthai REE deposit is best described as a low temperature carbothermalite microbreccia consisting of a wide variety of clasts resulting from the autobrecciation of rocks formed during, and after, the magmatic to carbothermal transition of an undetermined parental carbonatite-forming magma. Many clasts have been replaced by late stage

La-enriched carbothermal fluids mixed with exogenous water during the final low temperature stage of evolution of the deposit.

2. Daqingshanite at Kamthai occurs as two paragenetic types: primary granular coarse grained and coexisting with primary carbocernaite and barite and bastnäsite; and micro-ovoid globules of as yet undetermined origin.

3. Carbocernaite forming trellis-type lamellae in Sr-calcite clasts does not represent exsolution and is considered as a replacement texture.

### Acknowledgements

This research was supported by Lakehead University and Almaz Petrology. Ramgad Minerals and Dr. S. K. Bhushan are thanked for providing samples of the Kamthai REE deposit. The reviewers are thanked for constructive critiques of this study. Valerie Dennison is thanked for editorial assistance. Principal Editor and Production Manger Stuart Mills and Helen Kerbey, respectively, are thanked for editorial handing of this contribution.

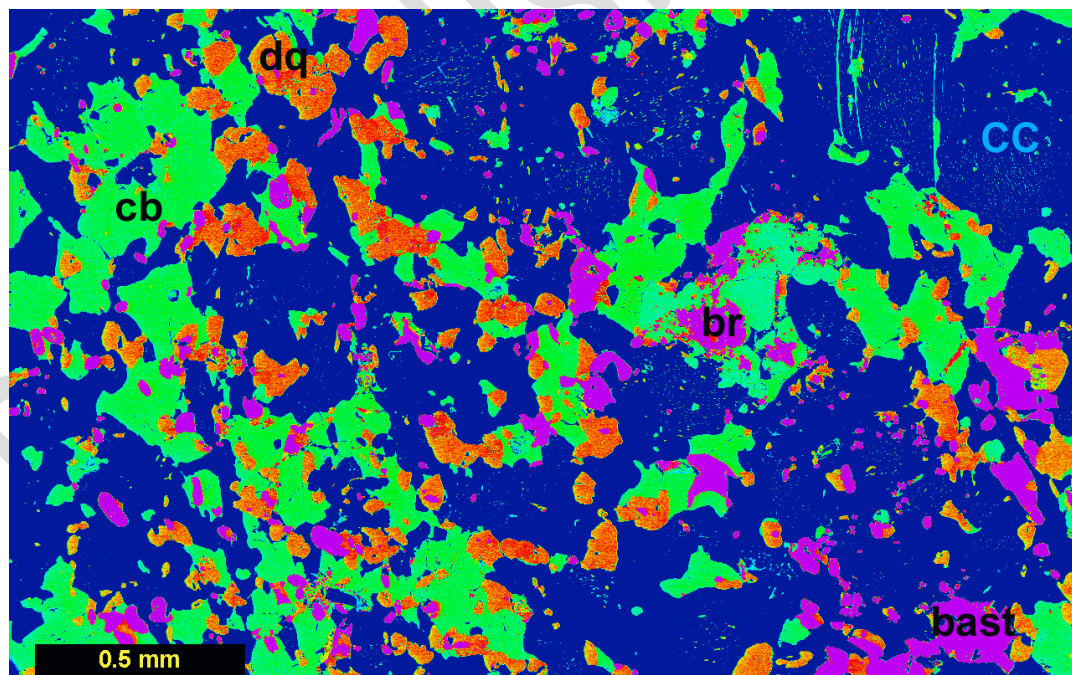


**Fig. 1.** Paragenetic relationships between britholite (br), daqingshanite (dq), and carbocernaite (cb). False colour BSE-image empathizing the sequence of crystallization of these three minerals. All are set in an colour-undifferentiated matrix of diverse calcite (cc).

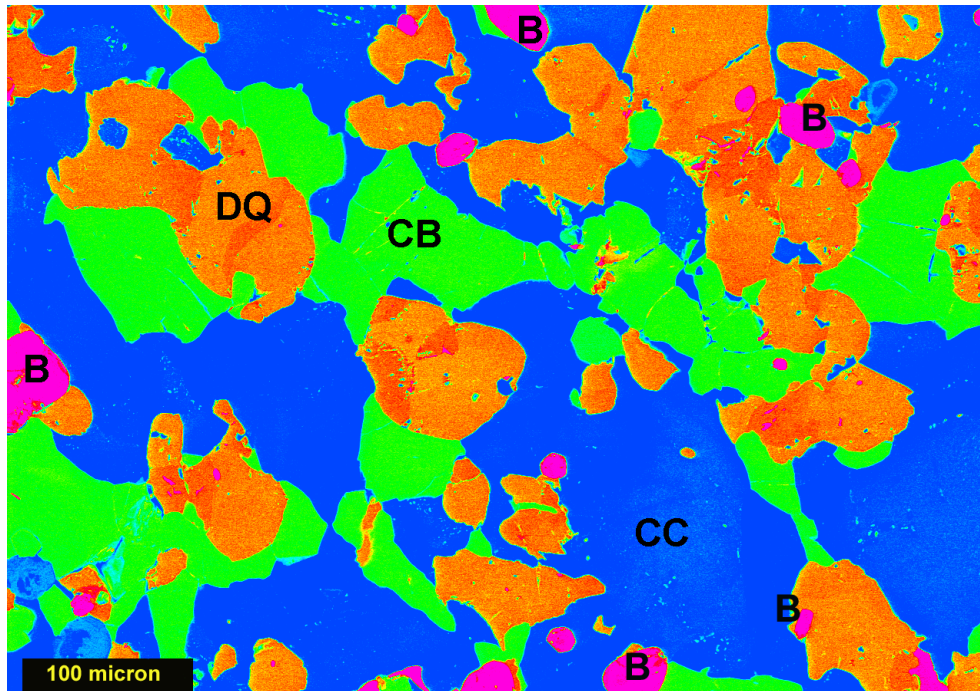


**Fig. 2.** False colour BSE-image of anhedral, resorbed and compositionally zoned coarse grained daqingshanite (DQ) overgrown by carbocernaite (CB) of uniform composition set in an colour-undifferentiated matrix of diverse calcite (CC).

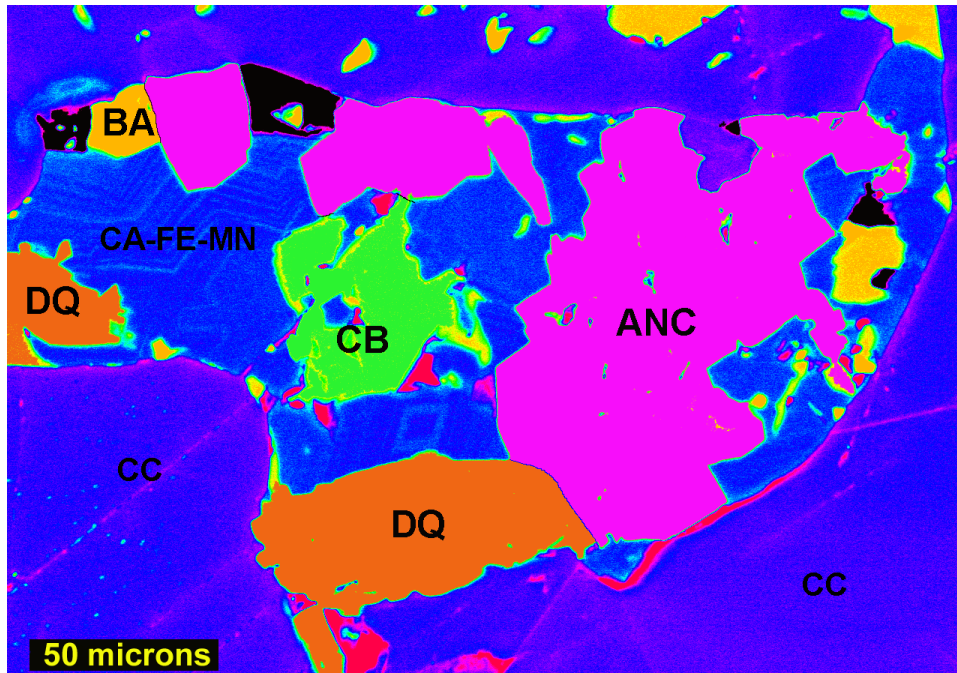


**Fig. 3.** False colour BSE-image of a clast showing the paragenetic relationships between early-formed daqingshanite (DQ) and carbocernaite (CB) set in a matrix of ancylite (ANC), barite (BAR) and Ca-Fe-Mn carbonates of diverse composition. The clast is set in matrix of Sr-poor calcite (CC).

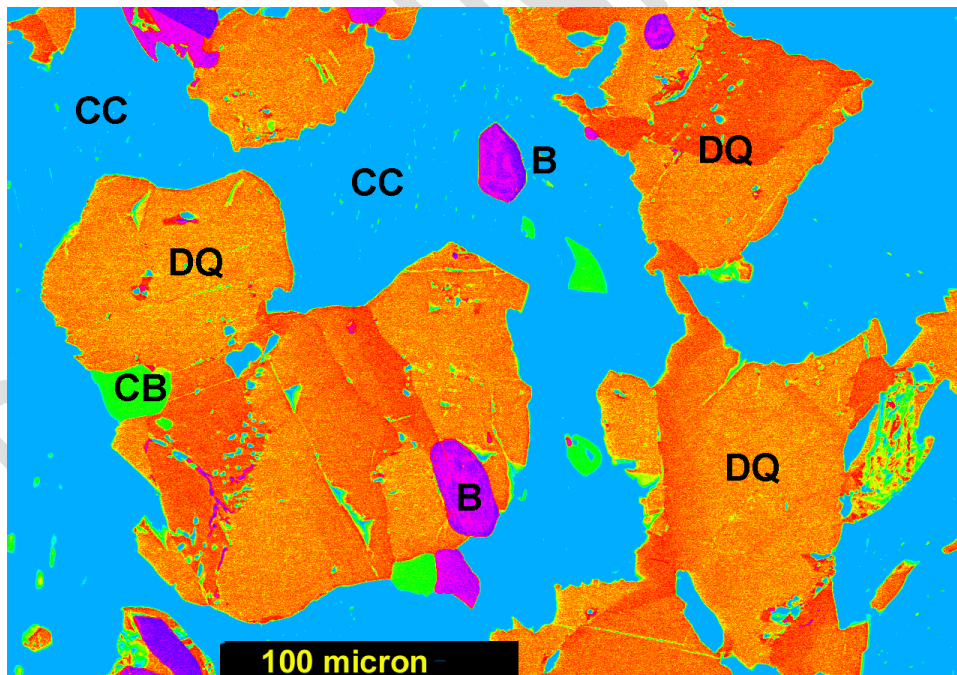


**Fig.4.** False colour BSE-image illustrating the compositional zoning in primary granular daqingshanite.

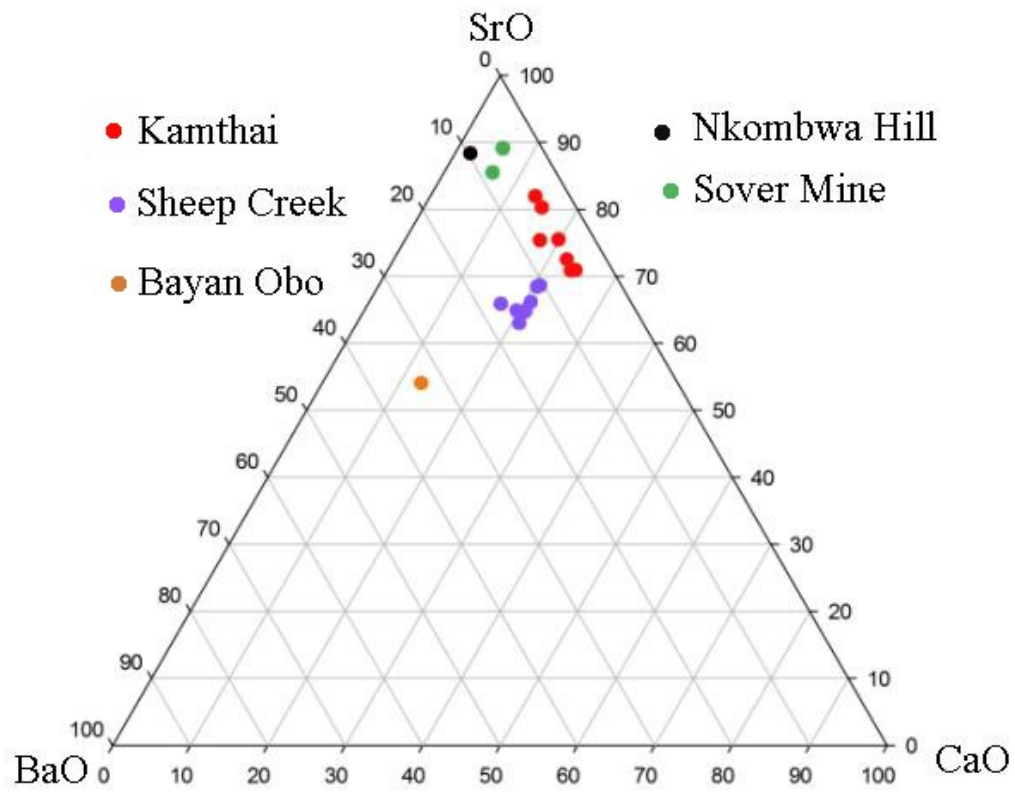


**Fig. 5** Compositions of daqingshanite expressed in the ternary system CaO-SrO-BaO. Data from: this work; Yingchen et al. (1983); Wall, et al. (1993); Appleton et al. (1992); Mitchell (1996); and Risedorf (2023)

Preprint

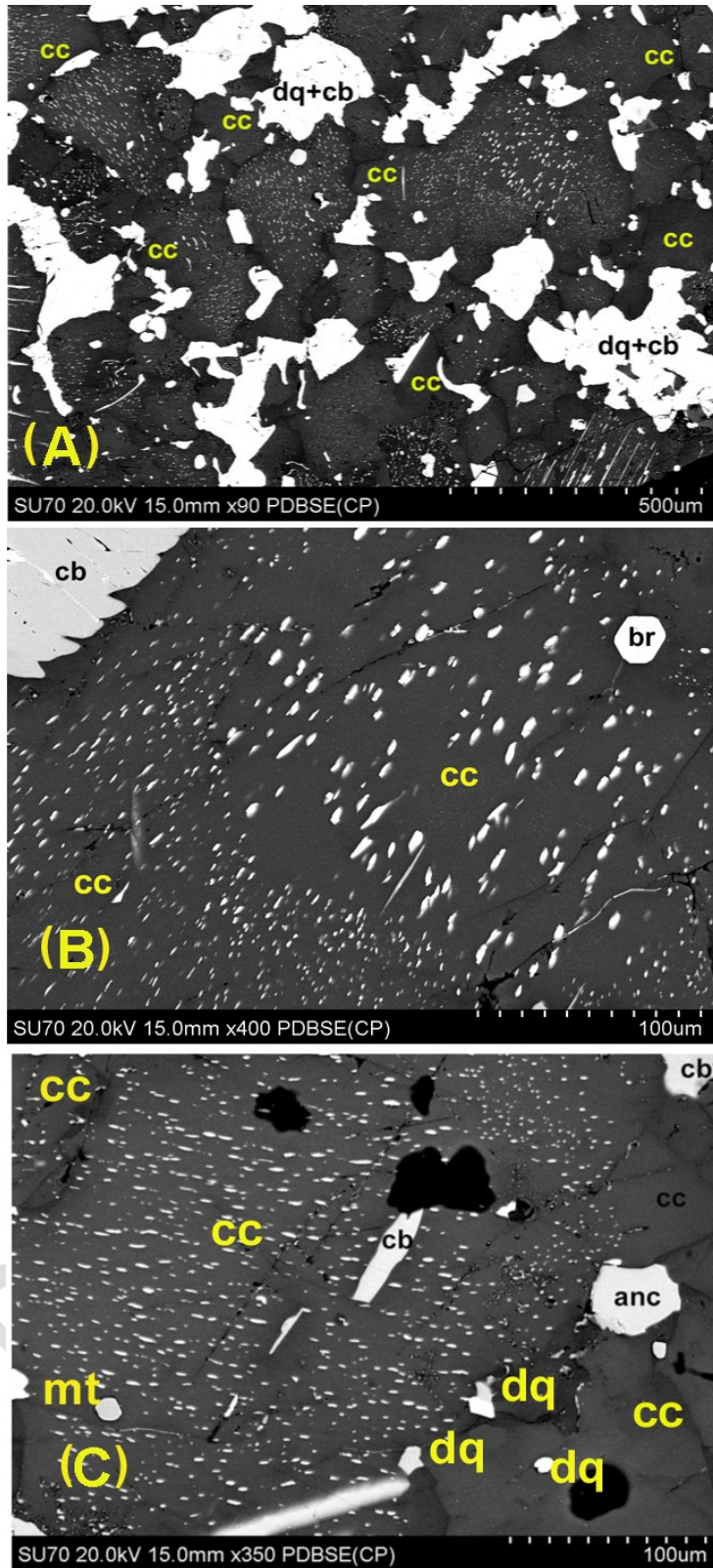
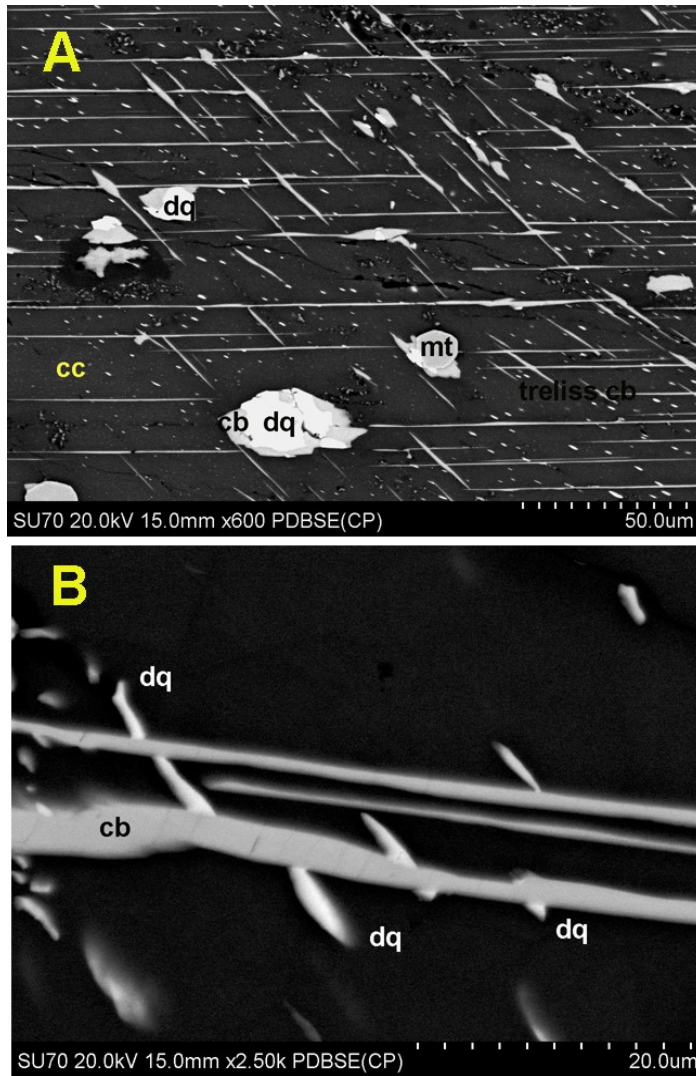


Fig. 6. BSE-images of: (A) Microbreccia with clasts of type 2 daqingshanite plus carbocernaite (dq+cb), and clasts of



type 2 micro-globular daqingshanite set in a Sr-calcite matrix. All clasts are cemented in a matrix of Sr-calcite; (B) Composite clast of micro-globular type 2 daqingshanite (white) set in Sr-calcite (cc) with isolated antecryst of resorbed britholite (br); (C) Clast of micro-globular daqingshanite (white) set in Sr-calcite containing antecrystal carbocernaite (cb). The clast is set in a cement of Sr-calcite which contains resorbed antecrysts of granular type 1 daqingshanite (dq) and ancylite (anc).

Prepublished Article



**Fig. 7.** BSE-images of: (A) lamellae carbocernaite and micro-globular type 2 daqingshanite set in Sr-calcite matrix with resorbed antecrysts of type 1 daqingshanite (dq), carbocernaite (cb) and magnetite (mt). Note that the orientation of the daqingshanite ovoids is not the same as that of the carbocernaite lamellae: (B) Illustration of carbocernaite lamella cross-cutting micro-ovoids of type 2 daqingshanite. Dark matrix is Sr-calcite.

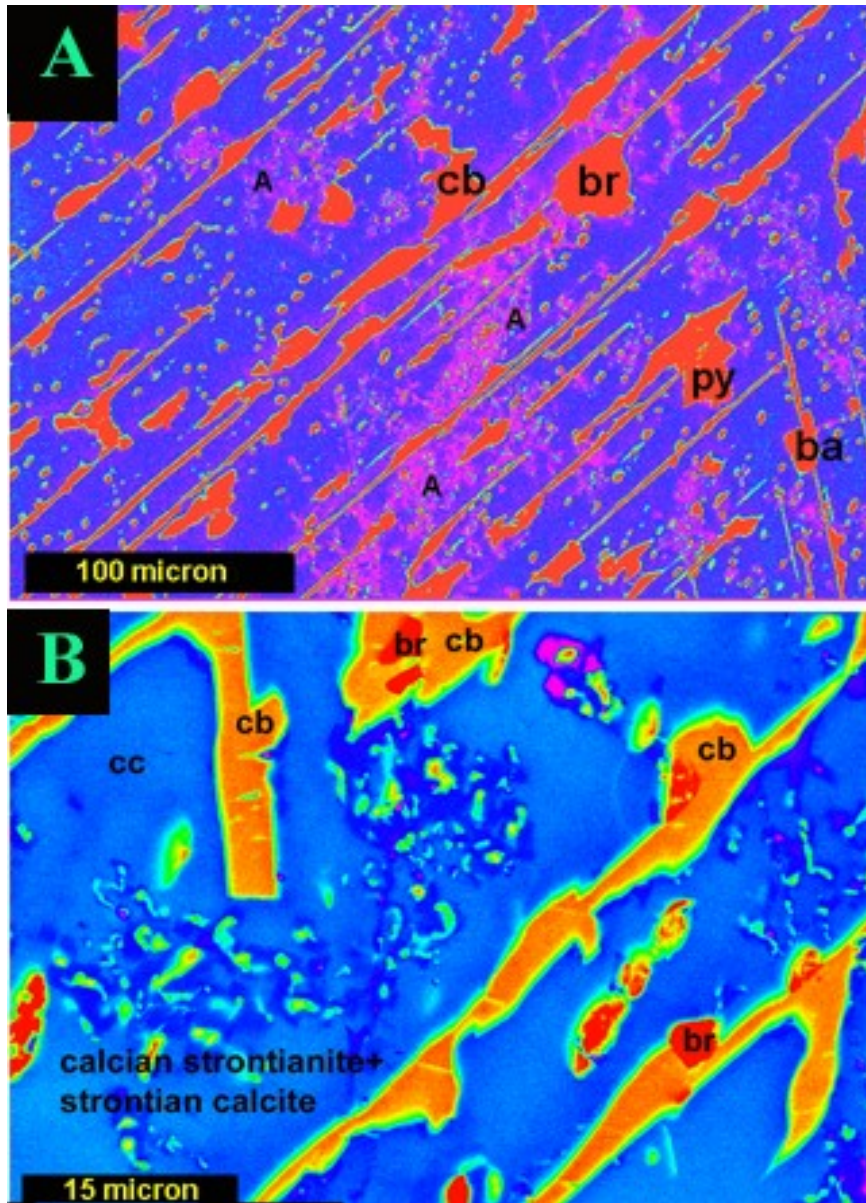


**Fig. 8.** False colour BSE-images of: (A) Replacement carbocearnite lamellae (cb) with antecrystal britholite (br), pyrite (py) and barite (ba) set in a Sr-calcite matrix showing secondary replacement textures (A); (B) Detail of the secondary replacements showing that they are composed of an intimate intergrowth of calcian strontianite (green) and strontian calcite (dark blue). Also present are carbocearnite lamella (cb) showing replacement textures with matrix calcite (cc) and antecrysts of britholite which have been transported with carbocearnite during the emplacement of the lamellae.

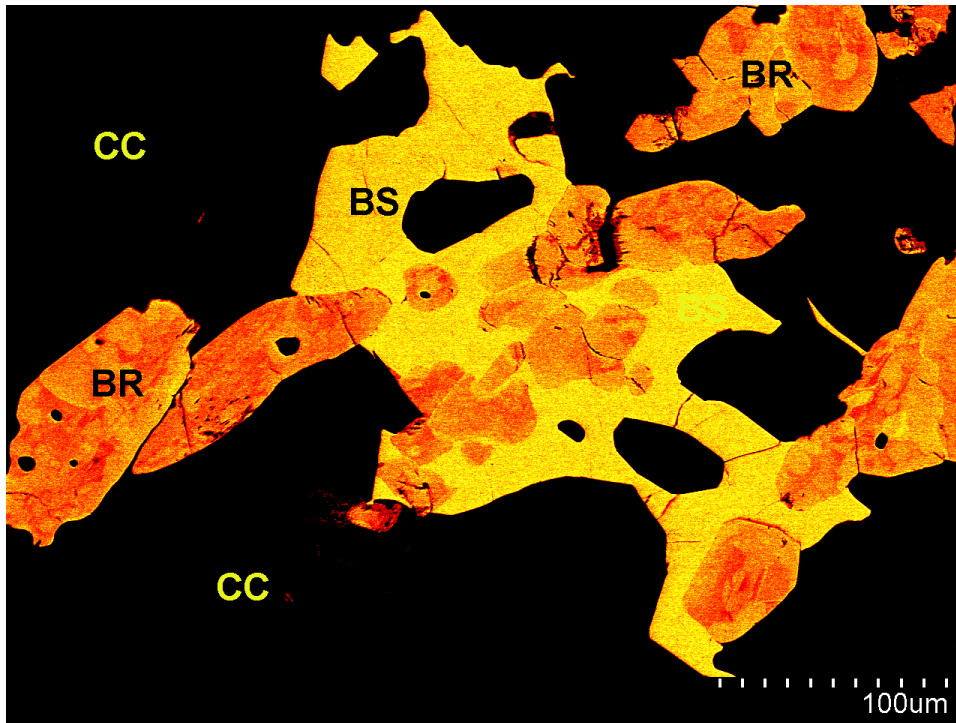


**Fig. 9.** False colour BSE-image of resorbed and compositionally zoned britholite set in a matrix of bastnäsite (bs) and calcite (cc).

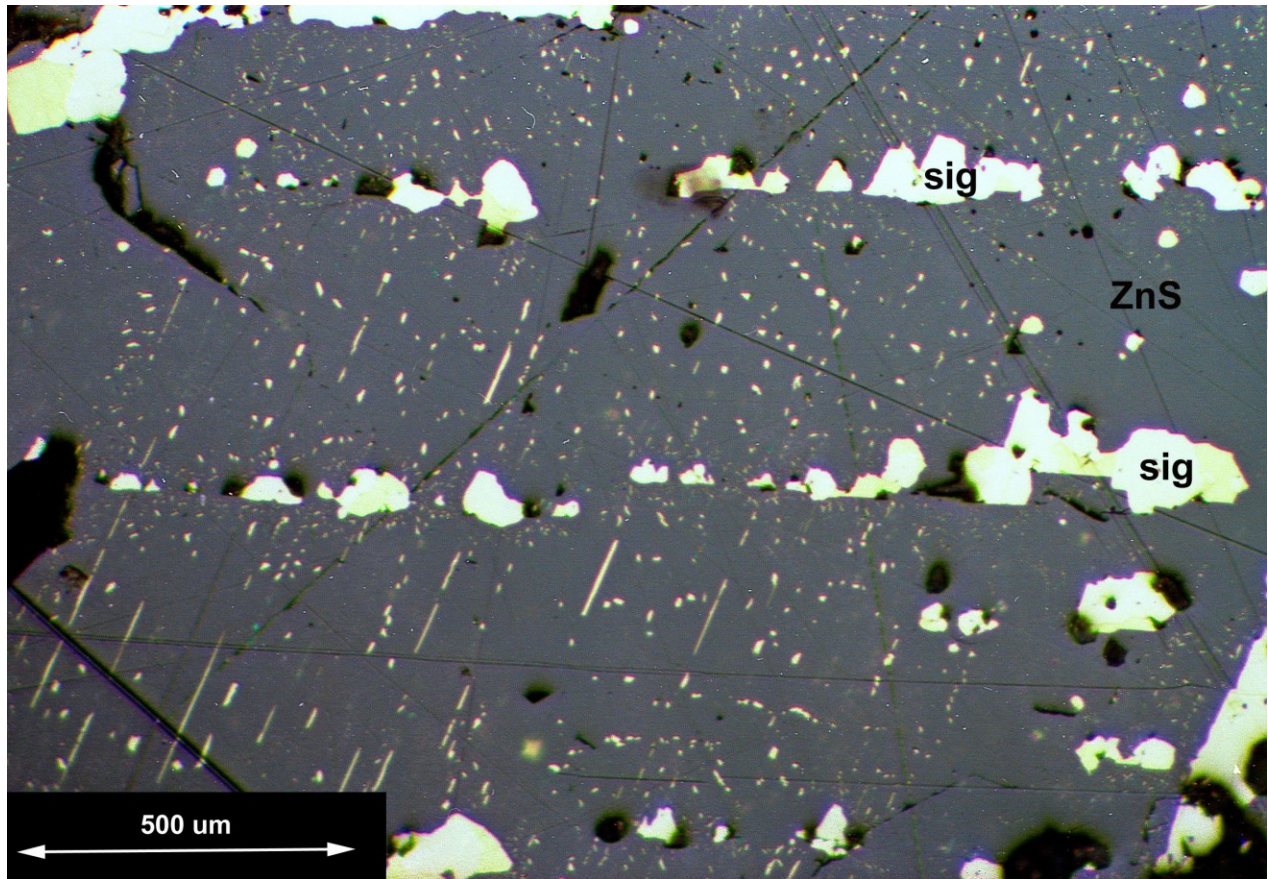


**Fig. 10.** Reflected light image of “chalcopyrite disease” which consists of micro-globular chalcopyrite (pale yellow) set in a matrix of sphalerite (ZnS). The coarse grained material is siegenite (sig). Compare the texture with that of daqingshanite illustrated in Fig. 6 of this work. This example of “chalcopyrite disease” is from the Erglodd Mine Mid-Wales (Image courtesy of Dr. John Mason and the Museum of Wales).

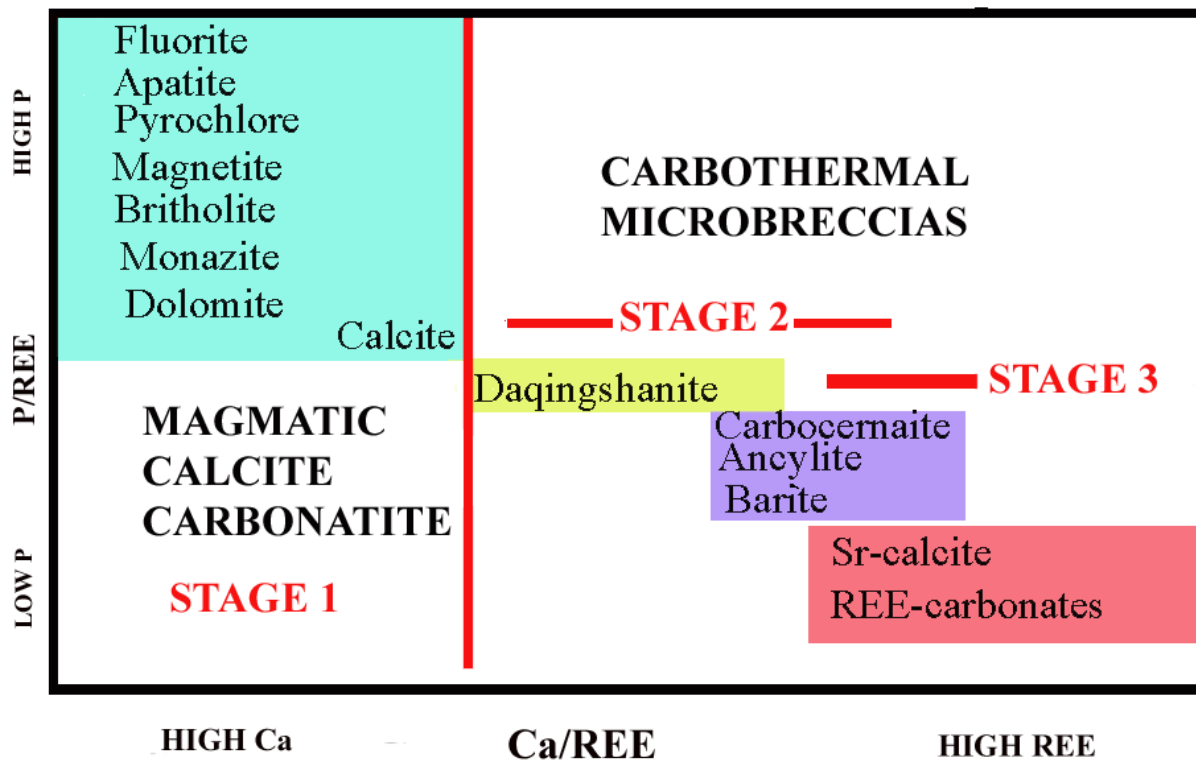
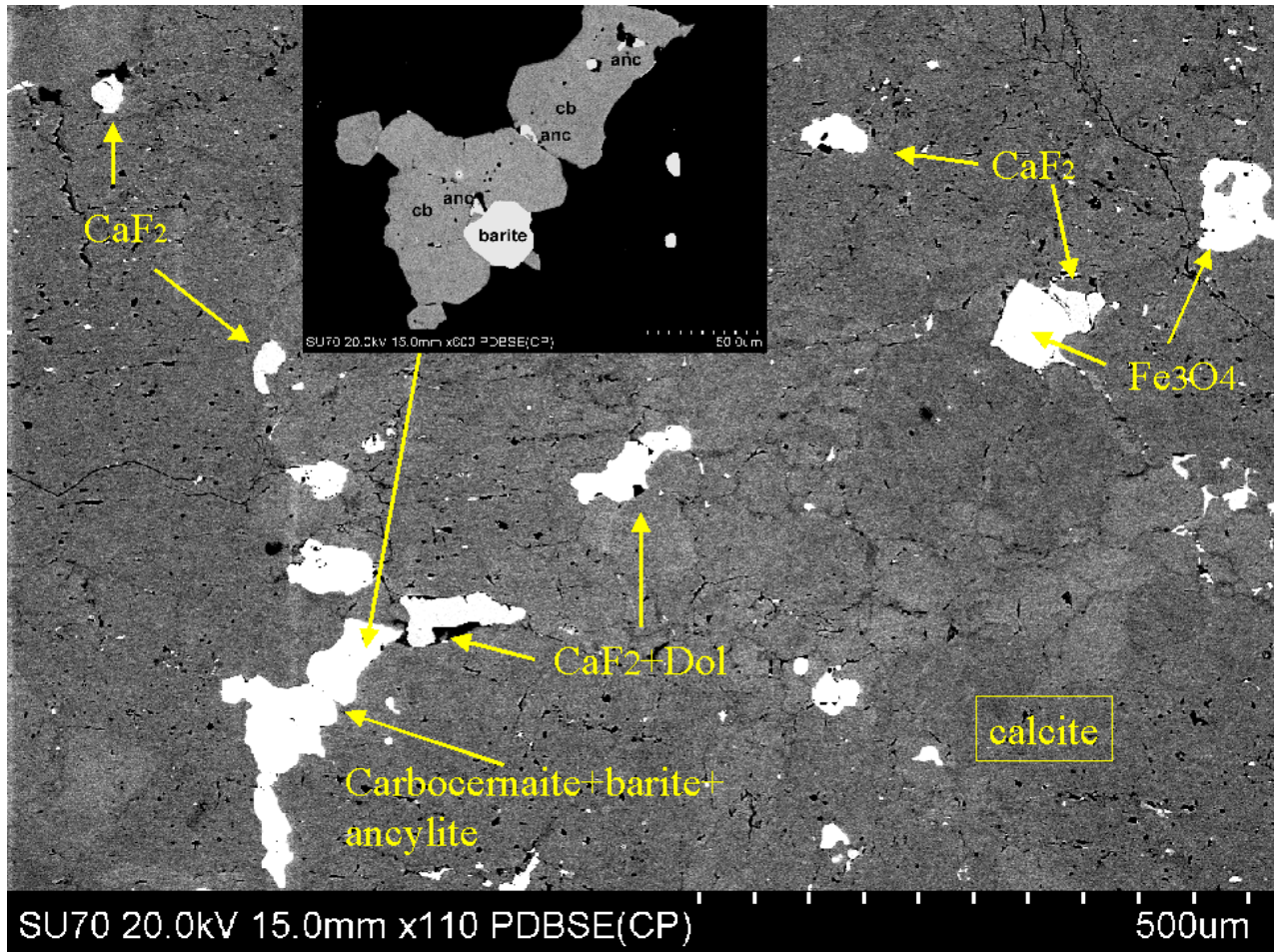
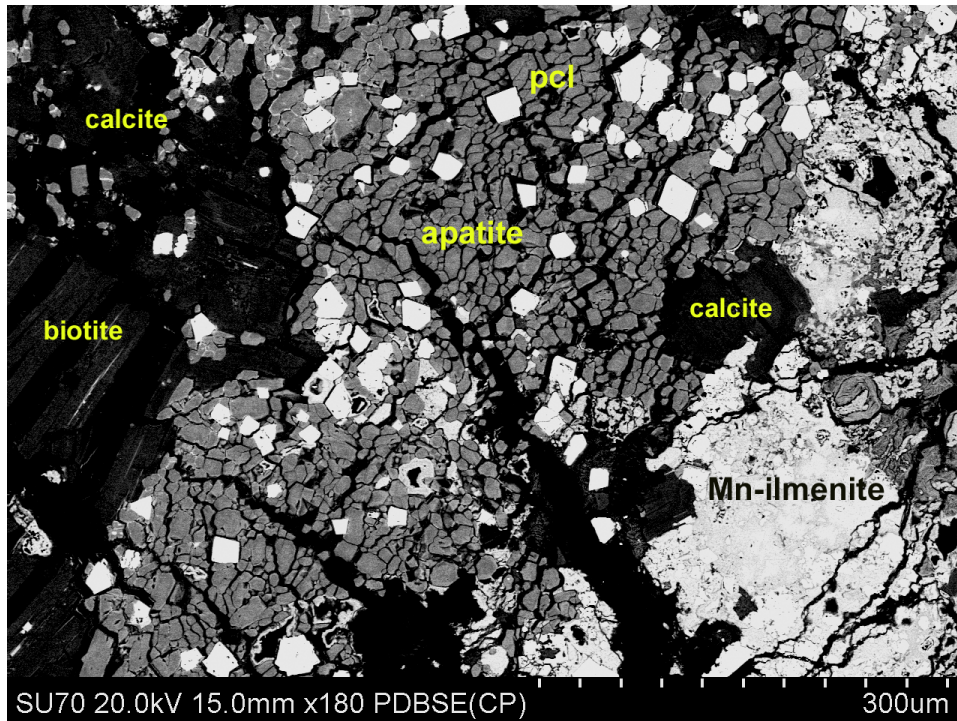


Fig.11. Paragenetic sequence of mineral assemblages in the stages of the evolution of the Kamthai carbothermal

Prepubl



**Fig. 12.** BSE-image of primary calcite carbonatite with late stage fluorite, carbocernaite, barite and ancylite (see the inset). Primary magnetite is also present. Note that the primary calcite exhibits variable but minor compositional variation as shown by the differing BSE-contrast. Dolomite is present in trace amounts.



**Fig.13.** BSE-image of pyrochlore (pcl) apatite clast undergoing disaggregation during formation of stage 3 carbothermalite microbreccia. The clast, now set in secondary carbo(hydro)thermal calcite, is derived from stage 1 primary calcite carbonatite. Also present are secondary biotite and Mn-ilmenite.



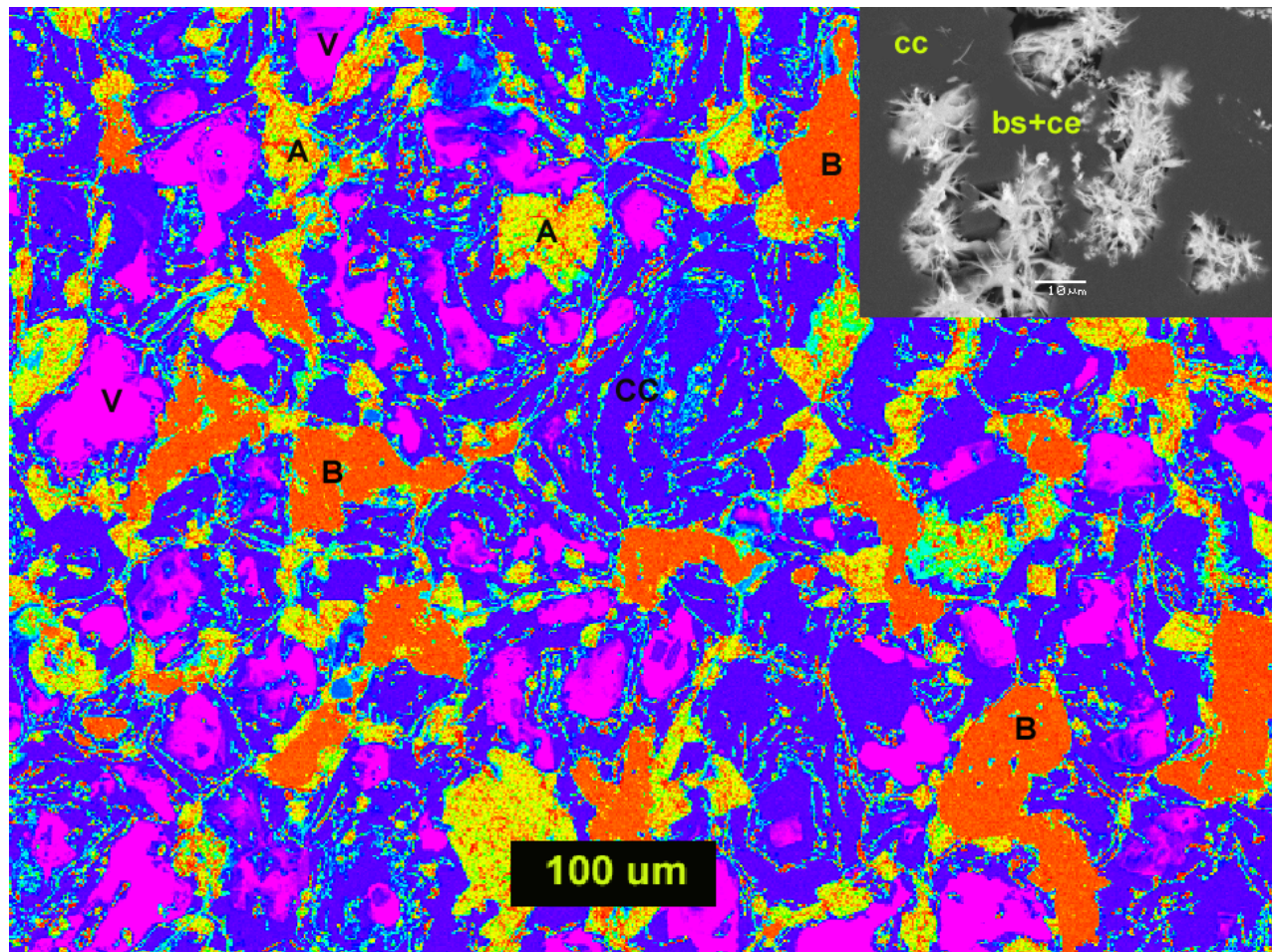


**Fig 14.** False colour BSE image of the texture of typical stage 3 carbothermalite microbreccia with clasts of stage 2 barite (B) and ancylite (ANC) set in porous (V) very complex stage 3 matrix of diverse Mn-Sr carbonates and iron oxide/hydroxides with fine grained REE-minerals including bastnäsite-(La), synchysite-(La) and cerite (see inset) .

#### References

- Amores-Casals S., Gonçalves A.O., Melgarejo J.C. and Molist J.M. (2020). Nb and REE distribution in the Monte Verde carbonatite-alkaline-agpaitic complex (Angola) *Minerals*, **2020**, 10,5;doi:10.3390/min100100005
- Appleton J.D., Bland D.J., Nancarrow P.H., Styles M.T., Mambwe S.H. and Zambezi P. (1992).The occurrence of daqingshanite-(Ce) in the Nkombwa Hill carbonatite, Zambia. *Mineralogical Magazine*, **56**, 419-422.
- Audétat A. and Edmonds M. (2020) Magmatic-Hydrothermal fluids. *Elements*, **16**, 401-406.
- Barker D.S., Mitchell R.H. and McKay D. (1987) Late Cretaceous nephelinite to phonolite magmatism in the Balcones province, Texas. Geological Society of America Special Paper 215, 293-304.
- Barton P.B. and Bethke P.M. (1987) Chalcopyrite disease in sphalerite: Pathology and epidemiology. *American Mineralogist*, **72**, 451-467.

- Bushan S.K. (2015) Geology of the Kamthai rare earth deposit. *Journal of the Geological Society of India*, **85**, 537-546.
- Bhushan S.K. and Kumar A. (2013) First carbonatite hosted REE deposit from India. *Journal of the Geological Society of India*, **81**, 41-60.
- Chebotarev D.A., Wohlgemuth-Überwasser C. and Tong H. (2022). Partitioning of REE between calcite and carbonatitic melt containing P, S, Si at 650-900°C and 100MPa. *Scientific Reports*, **12**:3320
- Chakhmouradian A.R., Cooper M.A., Reguir E.P. and Moore M.A. (2017). Carbocernaite from Bear Lodge, Wyoming: Crystal chemistry, paragenesis and rare-earth fractionation on a microscale. *American Mineralogist*, **102**, 1340-1352.
- Dowman E., Wall F. and Treloar P. (2022). A comparison of the fenites at the Chilwa Island and Kangankunde carbonatite complexes, Malawi. *Mineralogical Magazine*, **87**, 300-322.
- Engelhardt W. and Weiskirchner W. (1963) Einführung zu den Exkursionen der Deutschen Mineralogischen Gesellschaft zu den Vulkanschloten der Schwäbischen Alb und in den Hegau. *Fortschritte der Mineralogie*, **40**, 5-28.
- Haggerty, S.E. (1996) Oxide textures: a mini-atlas. *Reviews in Mineralogy and Geochemistry*, **25**, 125-219.
- Hughes J.M. and Yunxiang N. A high-precision crystal structure refinement of daqingshanite-(Ce) from the Nkombwa Hill carbonatite, Zambia. *Mineralogical Magazine*, **58**, 493-496.
- Mahala M.K. and Ray J.S. 2022. Age and geochemistry of the Kamthai carbonatites, Rajasthan, western India. *EGU General Assembly 2022 Vienna Austria*, EGU22-10951: doi.org/10.5194/egusphere-egu22-105551, 2022
- Louvel M., Etschmann, B., Qiushi G., Testemale D. and Brugger J. (2022) Carbonate complexation enhances transport of rare earth elements in alkaline fluids. *Nature Communications*: doi.org/10.1038/s414667-022-28888943-z
- Mitchell, R.H. (1995) *Kimberlites, Orangeites and Related Rocks*. Plenum Press, New York.
- Mitchell R.H. (2005) Carbonatites and carbonatites and carbonatites. *The Canadian Mineralogist*, **43**, 2049-2068.
- Mitchell R.H. and Gittins J. (2022) Carbonatites and carbothemalite: A revised classification. *Lithos* **430**: 106861, doi:10.1016/j.lithos.2022.106861.
- Mitchell R.H. and Platt R.G. (1984). The Freemans Cove volcanic suite: field relations, petrochemistry and tectonic setting of nephelinite-basanite volcanism associated with rifting in the Canadian Arctic archipelago. *Canadian Journal of Earth Sciences*, **21**, 428-436.
- Mitchell R.H., Wahl R. and Cohen H. (2020) Mineralogy and genesis of pyrochlore apatite from the Good Hope carbonatite, Ontario: A potential niobium deposit. *Mineralogical Magazine*, **84**, 81-91
- Molle V., Gaillard F., Nabyl Z., Tuduri J., Di Carlo I. (2021). Crystallization sequence of a REE-rich carbonatite melt: an experimental approach. *Comptes Rendus Géoscience - Series de la Planète*, **353**, 217-231
- Nagase T. and Kojima S. (1997) A SEM examination of the chalcopyrite disease texture and its genetic implications. *Mineralogical Magazine*, **61**, 80-97.
- Patel A.K. Upadhyay D., Mishra B. and Pruseth K.L. (2023a) Reconstruction of hydrothermal fluid composition of the Kamthai carbonatite complex, India using a lattice strain model: Implications for LREE/HREE fractionation.

*Lithos*, **444-445**, (2023) 107097.

- Patel A.K. Upadhyay D., Mishra B. and Pruseth K.L. (2023b) Magmatic rare earth mineralization and secondary fluid-assisted redistribution in the Kamthai carbonatite complex, NW India. *Lithos*, **456-457**, (2023) 107294.
- Perry E.P. and Gysi A.P. (2018) Rare earth elements in mineral deposits: speciation in hydrothermal fluids and partitioning in calcite. *Geofluids*:doi.org/10.1155/2018/5382480
- Risedorf S. (2023) Investigations of the Sheep Creek carbonatite, Ravelli County, Montana. Montana Technical University Butte, Montana. Unpublished M.Sc. Thesis. 151 pp.
- Ronchi L.H., Basos Neto A.C., Gedoz S.C., Weber M.L., Pereira V.P. and Andrek M. (2011) A transção magmático-hidrotermal registra por inclusões no albitó-granito de núcleo Mina Pitinga, Amazonas. Pp 71-88 In Contribuições a Metalica do Brasil. (J.C. Frantz, J.M., Charão J.M. and H. Jost, editors)
- Shi N., Ma Z. and Peng Z. (1982) The crystal structure of carbocearnite. *Kexue Tongbao* **27**, 76-80 (In Chinese).
- Sitnikova M.A., Do Cabo V., Wall, F. and Goldmann S. (2021). Burbankite and pseudomorphs from the Main intrusion calcite carbonatite, Lofdal, Namibia: Association, mineral composition and Raman spectroscopy. *Mineralogical Magazine*, **85**, 496-513.
- Tun M.M. and Aye M.T. (2020) Origin of chalcopyrite disease from lead-zinc-silver-gold mineralization of the Scharchet area, Thabeikkyin Township, Mandalay Region, Myanmar. *International Journal of Scientific Research in Multi disciplinary Studies*, **6**, 81-86.
- Upadhyay D., Monndal S., Patel A.K., Mishra B., Pruseth K.L. and Bhushan S.K.(2021). Rare earth element precipitation induced by non-redox transformation of magnetite to hematite: Microtextural and geochemical evidence from the Kamthai carbonatite complex, western India. *Lithos*, **400-401**, 106381.
- Wall F, and Mariano A.N. (1996) Rare earth minerals in carbonatites: a discussion centred on the Kangankunde Carbonatite, Malawi. Pp.193 –225 In *Rare Earth Minerals: Chemistry, Origin and Ore Deposits*. The Mineralogical Society Series 7. (A.P. Jones, F.Wall, and T.C. Williams, Editors. Chapman & Hall, London UK.
- Wall, F. and Zaitsev, A.N. (2004) Rare earth minerals in Kola carbonatites, Pp.341-373. In *Phoscorites and Carbonatites from Mantle to Mine: the Key Example of the Kola Alkaline Province*. (F.Wall and A.N. Zaitsev, editors). Mineralogical Series 10, Mineralogical Society, London UK.
- Wall F., Le Bas M.J. Srivastava R.K. (1993) Calcite and carbocearnite exsolution and eutectic textures in a Sr, REE-rich carbonatite dyke from Rajasthan, India. *Mineralogical Magazine*, **57**, 495-513.
- Ximen L. and Peng Z. (1985) Crystal structure of daqingshanite. *Geochemistry (China)*, **4**, 89-96.
- Yingchen R., Lulu X. and Zhizhong P. (1983) Daqingshanite - a new mineral recently discovered in China. *Geochemistry (China)*, **2**, 180-184.
- Zaitsev A.N., Wall F. and Le Bas M.J. (1998). REE-Sr-Ba minerals from the Khibina carbonatites, Kola Peninsula, Russia: their mineralogy, paragenesis and evolution. *Mineralogical Magazine*, **62**, 225-250.

Table 1. Representative compositions of daqingshanite

Wt.%	1	2	3	4	5	6	7	8	9
Na <sub>2</sub> O	0.36	0.40	0.48	0.26	bld	bld	bld	bld	0.13
K <sub>2</sub> O	0.49	0.46	0.50	0.34	0.34	0.19	bld	bld	bld
CaO	9.15	9.24	9.00	8.42	6.33	5.85	7.75	6.94	6.17
SrO	26.71	27.60	29.16	32.08	33.27	35.23	33.41	41.82	26.10
BaO	1.79	2.10	2.05	1.99	1.83	1.91	3.17	4.57	15.98
La <sub>2</sub> O <sub>3</sub>	11.57	13.60	12.22	10.54	11.75	11.25	10.97	10.22	7.88
Ce <sub>2</sub> O <sub>3</sub>	12.32	12.41	13.03	12.84	12.70	12.11	10.91	12.24	10.60
Pr <sub>2</sub> O <sub>3</sub>	0.79	0.90	0.99	1.02	0.98	0.71	bld	0.83	0.68
Nd <sub>2</sub> O <sub>3</sub>	1.53	1.44	1.75	1.92	1.51	1.79	1.53	1.71	1.59
P <sub>2</sub> O <sub>5</sub>	8.11	8.26	8.14	9.05	9.88	9.55	8.82	10.50	11.73
SO <sub>3</sub>	0.89	0.99	0.71	0.55	0.14	0.11	0.42	nd	nd
Total	74.11	77.40	78.63	79.01	78.73	78.70	76.78	82.82	80.86
Na	0.079	0.085	0.101	0.054	-	-	-	-	-
K	0.035	0.082	0.034	0.023	0.024	0.013	-	-	-
Ca	1.107	1.086	1.042	0.963	0.748	0.693	0.917	0.112	0.772
Sr	1.748	1.756	1.826	1.986	2.127	2.259	2.139	2.689	1.652
Ba	0.079	0.090	0.087	0.083	0.079	0.083	0.137	0.198	0.684
<i>A-site</i>	<i>3.048</i>	<i>3.050</i>	<i>3.090</i>	<i>3.109</i>	<i>2.977</i>	<i>3.048</i>	<i>3.193</i>	<i>2.988</i>	<i>3.086</i>
La	0.498	0.510	0.487	0.415	0.478	0.459	0.447	0.418	0.317
Ce	0.509	0.499	0.515	0.502	0.513	0.490	0.441	0.497	0.424
Pr	0.032	0.036	0.039	0.040	0.039	0.029	-	0.034	0.027
Nd	0.062	0.056	0.068	0.073	0.059	0.071	0.060	0.068	0.062
<i>B-site</i>	<i>1.102</i>	<i>1.101</i>	<i>1.109</i>	<i>1.030</i>	<i>1.089</i>	<i>1.048</i>	<i>0.948</i>	<i>1.106</i>	<i>0.830</i>
P	0.775	0.767	0.744	0.818	0.922	0.894	0.824	0.986	1.084

S	0.075	0.082	0.058	0.044	0.012	0.009	0.035	-	-
<i>C-site</i>	<i>0.850</i>	<i>0.849</i>	<i>0.802</i>	<i>0.862</i>	<i>0.934</i>	<i>0.903</i>	<i>0.859</i>	<i>0.986</i>	<i>1.084</i>

Structural formulae calculated on the basis of 5 cations.

Prepublished Article

Table 2. Composition of globular daqingshanite

Wt.%	1	2	3	4
Na <sub>2</sub> O	0.41	0.59	0.35	bld
K <sub>2</sub> O	0.62	0.97	0.72	0.22
CaO	8.49	7.83	11.01	11.22
SrO	27.92	30.03	30.19	32.92
BaO	2.34	3.03	2.35	1.94
La <sub>2</sub> O <sub>3</sub>	12.19	12.48	12.10	8.74
Ce <sub>2</sub> O <sub>3</sub>	11.64	12.83	11.97	11.58
Pr <sub>2</sub> O <sub>3</sub>	1.05	0.70	0.99	0.83
Nd <sub>2</sub> O <sub>3</sub>	1.36	1.35	1.36	1.96
P <sub>2</sub> O <sub>5</sub>	7.48	6.32	7.02	8.53
SO <sub>3</sub>	0.93	1.05	0.95	1.78
Total	74.43	77.18	79.01	79.72

Prepublished Article

Table 3. Representative composition of carbocernaite

wt.%	1	2	3	4	5	6	7	8	9	10	11
Na <sub>2</sub> O	3.25	3.43	3.54	3.80	3.97	3.40	3.50	3.77	0.44	2.84	4.11
CaO	16.53	16.88	16.48	16.44	15.75	16.43	16.96	16.39	15.59	14.89	16.95
SrO	23.90	22.66	24.23	21.59	20.89	21.72	22.67	21.88	24.45	19.95	21.36
BaO	1.13	1.09	1.18	0.98	0.82	1.34	1.71	1.45	0.98	0.20	1.44
La <sub>2</sub> O <sub>3</sub>	8.05	8.01	8.99	9.35	10.16	7.98	8.35	9.01	10.36	11.42	11.77
Ce <sub>2</sub> O <sub>3</sub>	8.40	8.91	9.82	9.67	10.18	9.23	9.02	9.86	11.39	14.20	9.72
Pr <sub>2</sub> O <sub>3</sub>	0.84	0.84	0.83	0.63	0.79	0.75	0.57	0.71	1.09	1.28	0.75
Nd <sub>2</sub> O <sub>3</sub>	1.33	0.95	0.88	0.92	0.80	1.07	0.72	0.91	1.97	2.46	1.98
Total	63.67	64.21	65.95	63.55	63.59	63.51	63.72	64.23	66.27	67.24	68.36
Na	0.278	0.294	0.293	0.324	0.340	0.296	0.297	0.320	0.037	0.237	0.329
Ca	0.780	0.799	0.753	0.774	0.746	0.791	0.796	0.768	0.733	0.686	0.750
<i>A-site</i>	1.058	1.093	1.046	1.098	1.086	1.087	1.093	1.088	0.770	0.923	1.079
Sr	0.610	0.580	0.599	0.550	0.536	0.566	0.576	0.555	0.692	0.498	0.512
Ba	0.020	0.019	0.020	0.017	0.014	0.024	0.029	0.025	0.017	0.003	0.023
La	0.131	0.131	0.141	0.152	0.166	0.132	0.135	0.145	0.168	0.181	0.179
Ce	0.135	0.144	0.153	0.156	0.165	0.152	0.145	0.158	0.190	0.224	0.147
Pr	0.013	0.014	0.013	0.010	0.013	0.012	0.009	0.011	0.017	0.020	0.011
Nd	0.021	0.015	0.013	0.014	0.013	0.017	0.011	0.014	0.031	0.038	0.029
<i>B-site</i>	0.930	0.903	0.939	0.899	0.907	0.903	0.905	0.908	1.115	0.964	0.901

Structural formulae calculated on the basis of 2 (CO<sub>3</sub>)<sup>2-</sup> groups. Compositions: 1-5 granular carbocernaite with daqingshanite; 6-8 lamella carbocernaite in calcite (this work); 9-10 from Patel et al. (2023); 11 granular carbocernaite with britholite (Wall et al. 1993).

Table 4. Representative compositions of britholite

wt.%	1	2	3	4	5	6	7	8	9
SiO <sub>2</sub>	17.99	18.67	18.96	16.78	17.36	16.86	24.20	20.21	18.39
P <sub>2</sub> O <sub>5</sub>	3.26	2.35	2.15	5.61	4.27	5.19	0.89	1.59	5.08
CaO	11.24	10.29	10.20	12.61	12.06	12.28	8.65	10.02	14.02
SrO	2.65	1.80	1.84	3.02	2.92	2.17	1.79	2.18	0.63
La <sub>2</sub> O <sub>3</sub>	15.01	16.91	17.17	16.47	14.69	16.58	18.87	21.47	23.71
Ce <sub>2</sub> O <sub>3</sub>	31.26	32.88	31.84	29.86	31.00	29.31	29.00	31.83	25.06
Pr <sub>2</sub> O <sub>3</sub>	3.22	3.06	3.25	2.92	3.16	3.42	2.60	2.64	1.29
Nd <sub>2</sub> O <sub>3</sub>	7.11	6.06	6.46	5.92	6.50	5.68	8.42	7.11	3.39
Sm <sub>2</sub> O <sub>3</sub>	0.85	0.98	1.09	0.95	0.72	0.89	0.72	-	-
F	0.89	0.90	0.39	1.04	0.75	0.85	1.52	2.00	0.15
Total	93.48	93.90	93.35	95.18	93.43	93.23	96.67	99.15	91.72
Si	2.602	2.735	2.776	2.343	2.477	2.404	3.393	2.851	2.551
P	0.399	0.291	0.267	0.663	0.516	0.627	0.107	0.202	0.597
<i>B-site</i>	3.001	3.026	3.043	3.006	2.992	3.031	3.500	3.053	3.147
Ca	1.742	1.615	1.600	0.848	1.843	1.876	1.300	1.514	2.083
Sr	0.222	0.153	0.156	0.440	0.420	0.179	0.146	0.178	0.051
La	0.801	0.914	0.927	0.848	0.773	0.872	0.976	1.117	1.213
Ce	1.655	1.763	1.707	1.526	1.619	1.530	1.489	1.644	1.273
Pr	0.170	0.163	0.173	0.149	0.164	0.178	0.133	0.136	0.065
Nd	0.367	0.317	0.338	0.295	0.331	0.289	0.422	0.358	0.168
Sm	0.042	0.049	0.055	0.046	0.035	0.044	0.035	-	-
<i>A-site</i>	4.999	4.974	4.957	4.994	5.008	4.969	4.500	4.947	4.853
F	0.407	0.417	0.181	0.459	0.338	0.383	0.624	0.892	0.066
F/OH	0.686	0.715	0.221	0.848	0.511	0.620	1.659	8.259	0.007

Structural formulae calculated on the basis of 8 cations. Compositions 1-3 are areas of high BSE contrast relative to areas 4-6 respectively (this work); 7 Wall et al. (1993) a average of 9 analyses; 8 “magmatic” and 9 altered britholite (Patel et al. 2023a )